Final Technical Report

USGS NEHRP Award G10AP00049

Characterizing Time-Dependent Slow Slip on the Cascadia Subduction Zone from GPS, Strainmeters, and Tide Gauges

David Schmidt (das@uoregon.edu*)
Ray Weldon (ray@uoregon.edu)
Dean Livelybrooks (dlivelyb@uoregon.edu)
Haiying Gao
Randy Krogstad
Sequoia Alba

Department of Geological Sciences
University of Oregon
1272 University of Oregon
Eugene, OR 97403-1272
Fax: 541-346-4692

* New contact info: dasc@uw.edu, 206-685-3799

Award Period: March 2010 through March 2011

Research supported by the U.S. Geological Survey (USGS), Department of the Interior, under USGS award number G10AP00049. The views and conclusions contained in this document are those of the authors and should not be interpreted as necessarily representing the official policies, either expressed or implied, of the U.S. Government.

Abstract

Slow slip events represent the transient release of strain in the transition zone of subduction systems. In this work, we characterize slow slip on the Cascadia subduction zone, and use this new insight to refine constraints on seismic hazards for the Pacific Northwest. In this work, we have expanded our existing catalog by examining slow slip events in 2009 and 2010. We have posted our slow slip catalog online and distributed source parameters for the community to utilize [Gao et al., 2012]. We have also considered strainmeter and tide gauge data in our analysis. We compare the observed strainmeter time series with predictions made by a GPS-derived slip model. We find qualitative agreement for some strainmeter stations. Discrepancies may be attributed to an in-exact slip model or calibration issues with the strainmeter data. We also explore the potential of using tide gauge records to observe the vertical deformation during slow slip events. We find that the regional pattern of uplift and subsidence can be resolved after appropriate filtering of common tidal fluctuations. This approach holds the potential of using tide gauge data on other subduction zone, particularly those without other geophysical instrumentation.

Introduction

Slow slip events provide insight into how strain is accumulated and released at the boundary of the kinematically locked up-dip and freely sliding down-dip portions of the plate interface. On the Cascadia subduction zone, these events occur over a period of several weeks where surface displacements show a westward drift of 2-5 mm oriented in the direction opposite to plate convergence. Both the surface displacement and tremor migration show a spatially and temporally correlated pattern suggestive of along-strike propagation [Dragert et al., 2001]. Recurrence intervals of slow slip events are on the order of months, which is short compared to the several-hundred-year recurrence interval for megathrust earthquakes on Cascadia. The short recurrence interval allows for multiple events to be observed and compared, to better understand how the kinematics vary in time and space.

The mapping of slow slip events along the subduction zone provides insight on the spatial and temporal pattern of strain release. First order questions include how source parameters vary along-strike and what percentage of the plate convergence is released by large slow slip episodes at various locations. Additionally, the up-dip and down-dip limits of slow slip can be correlated with other geophysical data, such as porosity, temperature, and structure, in an effort to better understand the underlying processes that facilitate aseismic slip. Slow slip and tremor also constrain the lower edge of the seismogenic zone, a variable that is useful for seismic hazard studies, and event histories are an input into studies that explore the time-dependent loading of stress on the seismogenic zone [Mazzotti and Adams, 2004].

In this work, we expand our catalog of slow slip events in Cascadia. This information is used to better delineate the maximum possible depth of coseismic rupture. While observations from GPS provide our primary data set for studying slow slip, we also explore the use of strainmeter and tide gauge data as additional constraints.

Geodetic Analysis of Cascadia Slow Slip Events

We estimate slip along the slab interface during slow slip events (SSEs) by inverting GPS data using the Extended Network Inversion Filter (ENIF). This methodology, based on an extended Kalman filter, has been successfully used to estimate slip transients on the San Andreas fault [Murray and Segall, 2005], slow slip in Cascadia [McGuire and Segall, 2003], and slow earthquakes in Japan [Miyazaki et al., 2003]. The filter is based on the premise that tectonic deformation is spatially correlated between adjacent stations, whereas benchmark motions are uncorrelated. This information is used to filter out the uncorrelated trends and random noise, and estimate the coherent fault slip that best models the temporally and spatially correlated surface deformation. The algorithm is an iterative least-squares inversion where state variables (such as fault slip and benchmark motion) are predicted and updated for each epoch of a time series. Covariance information is propagated with each time step, providing a consistent statistical parameterization through time.

We have added four events to our catalog (Figure 1): April 2009 near the Olympic Peninsula (M_w 6.6), August 2009 in NW Oregon (Mw 6.6), February 2010 in SW Oregon (M_w 6.4), and August 2010 in the Puget Sound area (M_w 6.7). The resolution of slow slip in Oregon has historically been limited by the paucity of GPS stations. As PBO is now fully deployed, we are better able to constrain the SSEs in this section of the subduction zone. The Oregon SSE's provide the first constraint on where SSE's are located on this section of the subduction zone, namely along the eastern side of the Oregon coast range.

We can also compare the location of slow slip in Oregon with the position of the seismogenic zone as constrained by leveling data (Figure 2). Other studies have suggested that the locked zone and ETS zones abut each other in NW Washington [Chapman and Melbourne, 2009]. Here we find that the locked zone and ETS zones are spatially separated in Oregon. There are several implications of this result. Firstly, the separation of the SSEs and seismogenic zones in Oregon (compared to where they abut in Washington) suggests that the parameters (i.e. pore pressure, temperature) that control where locking and SSEs occur may be distinct for each process. For example, while clay content and/or down-dip temperature may hypothetically control the zone of seismogenic locking, pore pressure may be more critical in determining where slow slip occurs. And since temperature and pore pressure are generally independent of each other on the plate interface (although they may be linked in other ways), the location of locking and SSEs do not necessarily have the same spatial positioning at all locations along the subduction zone. Secondly, the lack of locking directly up-dip of SSEs in Oregon raises the question of how strain is released in the transition zone. In Washington, the transition zone overlaps with the up-dip edge of SSEs. This means that the strain budget within the transition zone is composed of strain accumulation or SSEs. In Oregon, a minimal amount of locking is occurring within the tail of the transition zone. And SSEs are positioned down-dip. Since no strain accumulation is inferred, then a major fraction of the plate motion must be released aseismically. The mode of strain release (steady or time-dependent) is currently uncharacterized, and will be the focus of future work.

Evaluating Borehole Strainmeter Data

More robust constraints for the spatial distribution of slip can be gained by utilizing multiple sources of geodetic data. Along with the extensive networks of GPS stations, PBO also maintains a network of borehole strainmeters in Cascadia. The strainmeters observations are independent and more sensitive than GPS. Borehole strainmeters are capable of measuring crustal strain with nano-scale precision over a period of hours to days. This sensitivity is orders-of-magnitude greater than strain values calculated from GPS data, which makes strainmeters a unique geodetic instrument for elucidating the behavior of SSEs.

By accounting for levels of noise and calibration errors, the sensitivity of strainmeter data can be incorporated into formal inversions and add a useful geodetic constraint for SSEs. The Gladwin Tensor Strainmeters (GTSMs) maintained by PBO consist of four extensometers that measure the change in diameter of the strainmeter casing. The strainmeters are secured in the borehole using an expansive grout which changes the elastic moduli and prevents a direct measurement of crustal strain. For this reason, borehole strainmeters must be calibrated using a known external source of strain. Current PBO calibration methods work well for strainmeters located in areas where the theoretical tide is accurately calculated using the SPOTL software package and where there is little effect from local ocean loading. Data from strainmeters located near the coast have higher levels of uncertainty due to the errors inherent in the calibration technique. Studies have shown that the expected strain from theoretical tides can differ by as much as 30% from surface-mounted strain measurements in these regions. It has been demonstrated that the signal produced by long-term transient signals, such as slow-slip, is best evaluated on a case-by-case basis.

Due to these uncertainties, understanding the capabilities and limitations of strainmeter data, especially in regards to the quantification of noise sources and identification of non-tectonic artifacts, is necessary for the data to be used in formal inversions. We have employed the method of power density spectra [Agnew, 1992] to analyze noise levels for several strainmeters in the PBO network. The power density spectra are used to obtain the signal-to-noise ratio as a function of sampling frequency for individual stations. Spectral analysis has shown that the noise spectra obeys a noise model where the amplitude is proportional to f^{-2} (Figure 3). The noise levels were then compared between strainmeters to identify noisey or problematic stations. We also use these noise spectra plots to constrain the power of the noise (i.e. frequency dependent uncertainties) used to weight the data in kinematic inversions.

We have also verified the SSE signal recorded on several strainmeters. Strainmeter observations are compared to calculated strain transients to identify any discrepant values and to evaluate the accuracy of the calibration. Here we show a prediction of the strain rate field for the 2005 SSE (Figure 4). We use a slip model derived from the inversion of GPS time series, and then forward calculate the strain rate field observed at the earth's surface. This strainfield evolves in time as the SSE propagates along-strike. The time dependent evolution of the strain shows reasonably good agreement with the individual components of the strainmeter at B005 (Figure 5). Some stations (not shown) do not match the predicted strain signal, which likely suggests that there is some complexity in the rupture that is not represented in the slip model. With the resolution of noise levels, strainmeter time series data can now be incorporated into hyperparameter values and

used in the network inversion. Future work will focus on performing joint inversions with both GPS and strainmeter time series data.

Identifying Slow Slip Signals in Tide Gauge Data

Tide gauges record the vertical movement of the ocean surface relative to the land. Neighboring tide gauges are typically highly correlated along the coast as they experience a common tidal signal and ocean noise. However, the signals will vary if tectonic events cause a differential change in the height of the land. Thus by differencing tidal stations, it should be possible to isolate the relative uplift related to SSEs. With historical GPS data, it is challenging to resolve the transient displacement on the vertical component because of the noise level. An alternative measurement of vertical displacement is provided by tide gauges. In this work, we have developed a methodology for analyzing the tide gauge records and isolating the signature of slow slip.

We begin by removing the signal associated with the tides using NOAA's official prediction. The remaining signal is ocean and atmospheric noise that is generally associated with storms and is highly correlated between neighboring stations. We apply a frequency domain transfer function approach to filter out the coherent ocean noise between neighboring stations while leaving behind the relative uplift signal due to SSEs. Finally, the time series for two distant tide gauge stations are differenced. While the SSE is still at or below the level of the remaining noise, distant tidal stations often experience vertical displacement of the opposite sign during a SSE. Therefore, by differencing tidal stations, the signal-to-noise is enhanced. The full methodology, as well as a statistical and uncertainty analysis, is described in Alba [2011].

We examine the reduced tide gauge data for a 13-year period (1997-2010), and extract a 200-day window around the time of known slow slip events. For the larger slow slip events, we can identify a differential vertical offset between station pairs. To better resolve this signal, we also stack the time series for 12 SSEs (Figure 6). The stack suggests an average of 4-5 mm of differential vertical movement per SSE depending on the station pair, with calculated uncertainties of ~2 mm (Table 1). To cross-validate our results, we compare the differential uplift to a prediction using the slip distributions in our SSE catalog. The slip distributions are constrained by GPS data, and thus provide an independent estimate of differential uplift. The contours in Figure 6 map the predicted absolute uplift for an average of 11 SSEs. From this model prediction, Port Angeles (PA) is expected to uplift ~4 mm per event, while Port Townsend (PT) is expected to subside ~2 mm per event. Thus, the expected differential uplift between PA and PT is 6.2±1.8 mm per event, which is consistent with the observed differential uplift inferred from the tide gauges (5.1±1.4 mm).

While reducing the ocean noise in the tide gauge data is challenging, we have demonstrated that it is feasible . In regions where GPS networks are well established, the vertical component of GPS may be the preferred method to constrain the vertical deformation. However, tide gauges are relatively cheap instruments, are widely found along the world's coastlines, and have decades or centuries of historical data.

Publications resulting from this work

Gao, H., D. A. Schmidt, and R. Weldon (2012), Scaling relationships of source parameters for slow slip events, Bull. Seis. Soc. Am., 102, 1, 352-360, doi:10.1785/0120110096.

Public Dissemination of Slow Slip Catalog

http://faculty.washington.edu/dasc/site/research:catalog
http://faculty.washington.edu/dasc/BSSA/BSSA-D-11-00096_esupp.html

Cited References

Agnew, D. C. (1992), The time-domain behavior of power-law noises, *Geophys. Res. Lett.*, 19, DOI: 10.1029/91GL02832.

Alba, S. (2011), ETS in tidal records, M.S. thesis, University of Oregon, 75 p.

Boyarko, D. C., and M. R. Brudzinski (2010), Spatial and temporal patterns of nonvolcanic tremor along the southern Cascadia subduction zone, *J. Geophys. Res.,* 115, B00A22, doi:10.1029/2008JB006064.

Chapman, J. S., and T. I. Melbourne (2009), Future Cascadia megathrust rupture delineated by episodic tremor and slip, Geophys. Res. Lett., 36, L22301, doi:10.1029/2009GL040465.

Dragert, H., K. Wang, and T. S. James (2001), A silent slip event on the deeper Cascadia subduction interface, *Science,* 292, 1525-1528, DOI: 10.1126/science.1060152.

Gao, H., D. A. Schmidt, and R. Weldon (2012), Scaling relationships of source parameters for slow slip events, Bull. Seis. Soc. Am., 102, 1, 352-360, doi:10.1785/0120110096.

McGuire, J. J., and P. Segall (2003), Imaging of aseismic fault slip transients recorded by dense geodetic networks, *Geophys. J. Intl., 155*, 778-788.

Mazzotti, S., and J. Adams (2004), Variability of near-term probability for the next great earthquake on the Cascadia subduction zone, *Bull. Seism. Soc. Amer. , 94,* 1954-1959.

Miyazaki, S., J. J. McGuire, and P. Segall (2003), A transient subduction zone slip episode in southwest Japan observed by the nationwide GPS array, *J. Geophys. Res.,* 108, 2087, doi:10.1029/2001JB000456.

Murray, J. R., and P. Segall (2005), Spatiotemporal evolution of a transient slip event on the San Andreas fault near Parkfield, California, *J. Geophys. Res.,* 110, B09407, doi:10.1029/2005JB003651.

Figure and Tables

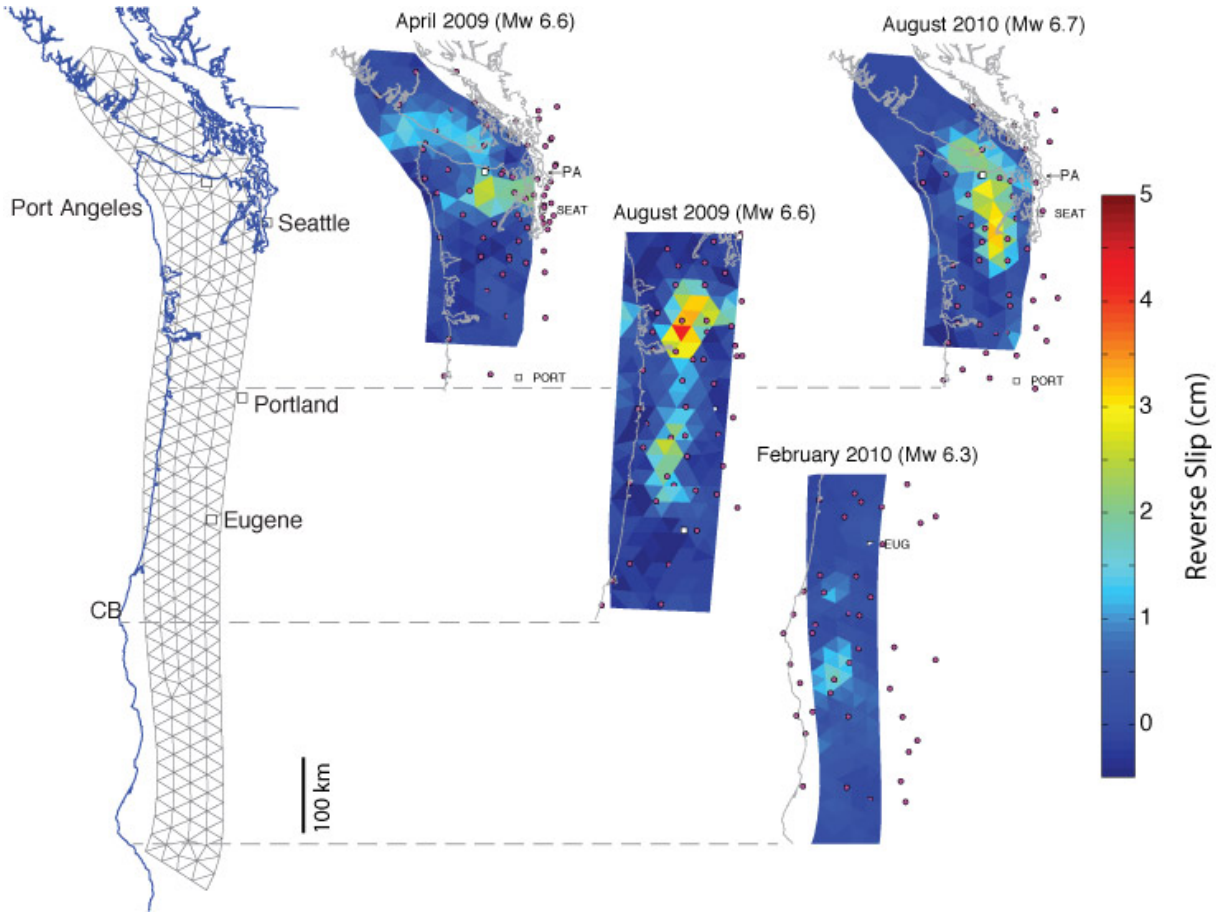

Figure 1 (Top): *New slip distributions for slow slip events in 2009 and 2010. Red dots indicate the location of GPS stations used in the analysis.*

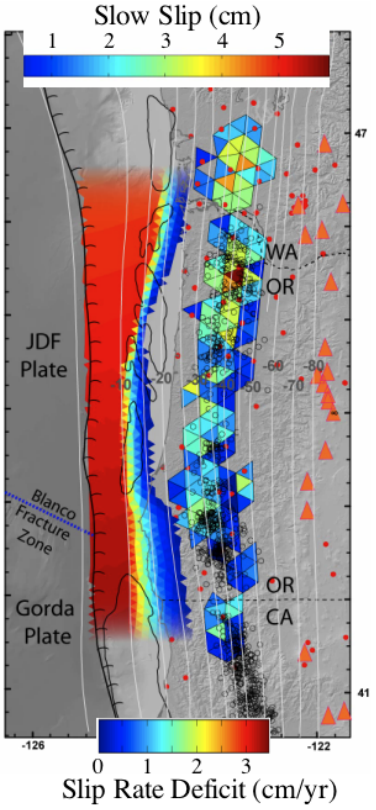

Figure 2 (Right): *The interseismic locking model for the central portion of the Cascadia subduction zone (colored field closest the trench; colorscale on the bottom) is compared to the spatial location of slow slip (colored triangles; colorscale on top) and tremor (black open circles; Boyarko and Brudzinski, 2010). Slow slip is shown as a mosaic of 3 separate Mw 6 events. Triangular slip patches are only displayed if the inferred slip on the plate interface is greater and 0.5 cm. In Oregon, we find a distinct separation in the interseismic locking model and the band of slow slip.*

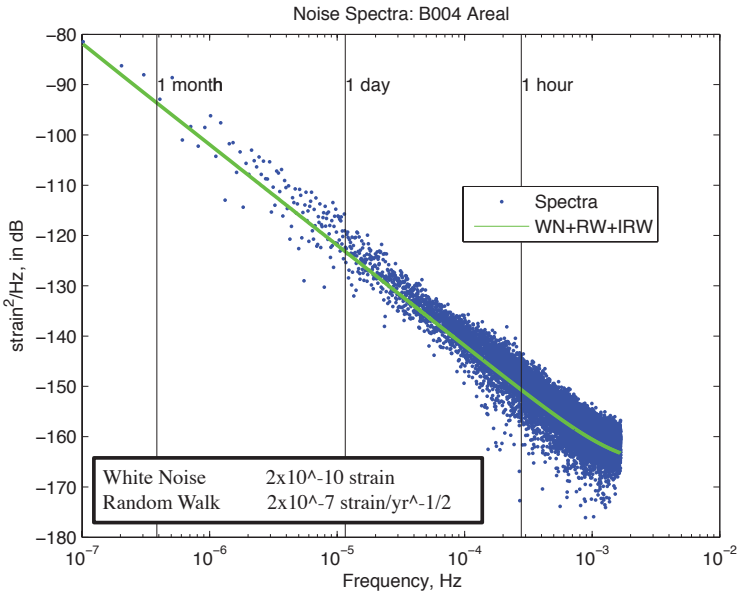

Figure 3: *Sample power density spectra of station B004 with the areal component of processed strain data shown. The green line represents the sum of the white noise and random walk values. Individual noise values are reported. This analysis shows strain data to predominately follow a random walk model for the sampling rate and duration chosen. 6 months of data sampled every five minutes was used in this analysis to correlate with the temporal span used in the slip inversion model. The data has been processed by PBO to remove nontectonic signals. The data was also selected during an interval with no known tectonic activity.*

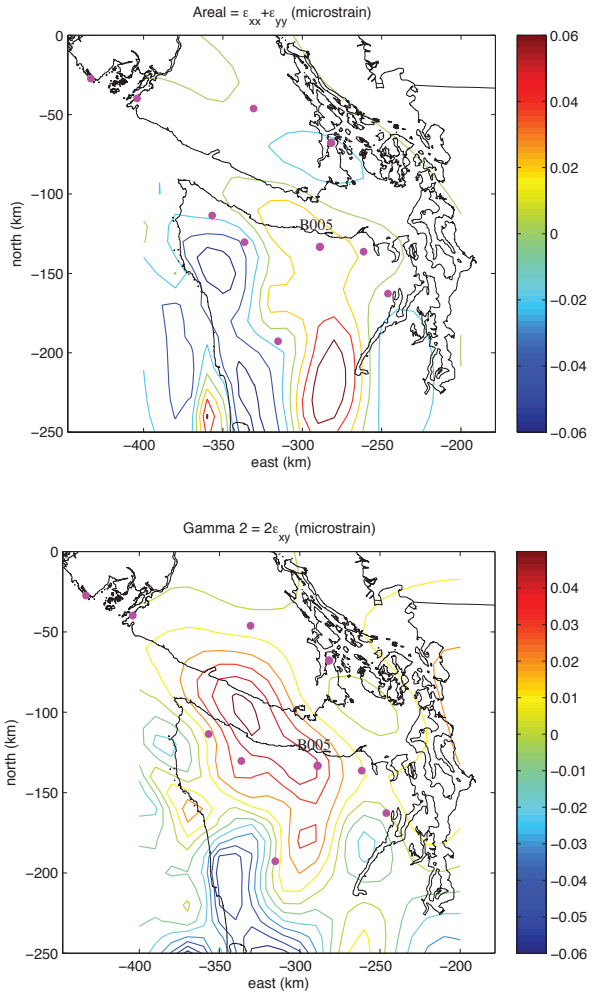

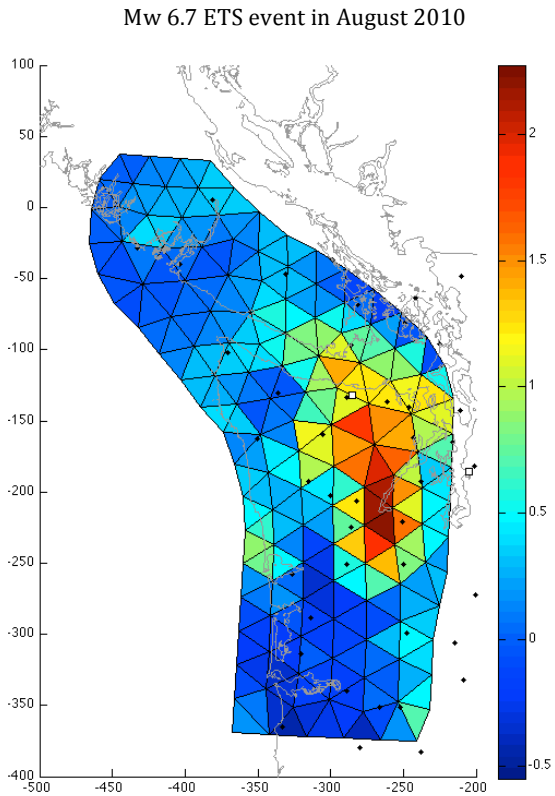

Figure 4: *Predicted strainfields (left column) for the August 2010 slow slip event using a GPS-derived slip model (upper right). Colored lines indicate net predicted strain change in microstrain. Magenta dots represent the strainmeter locations. For the slip distribution, the colorscale is in cm. Black dots show the GPS stations used in the inversion.*

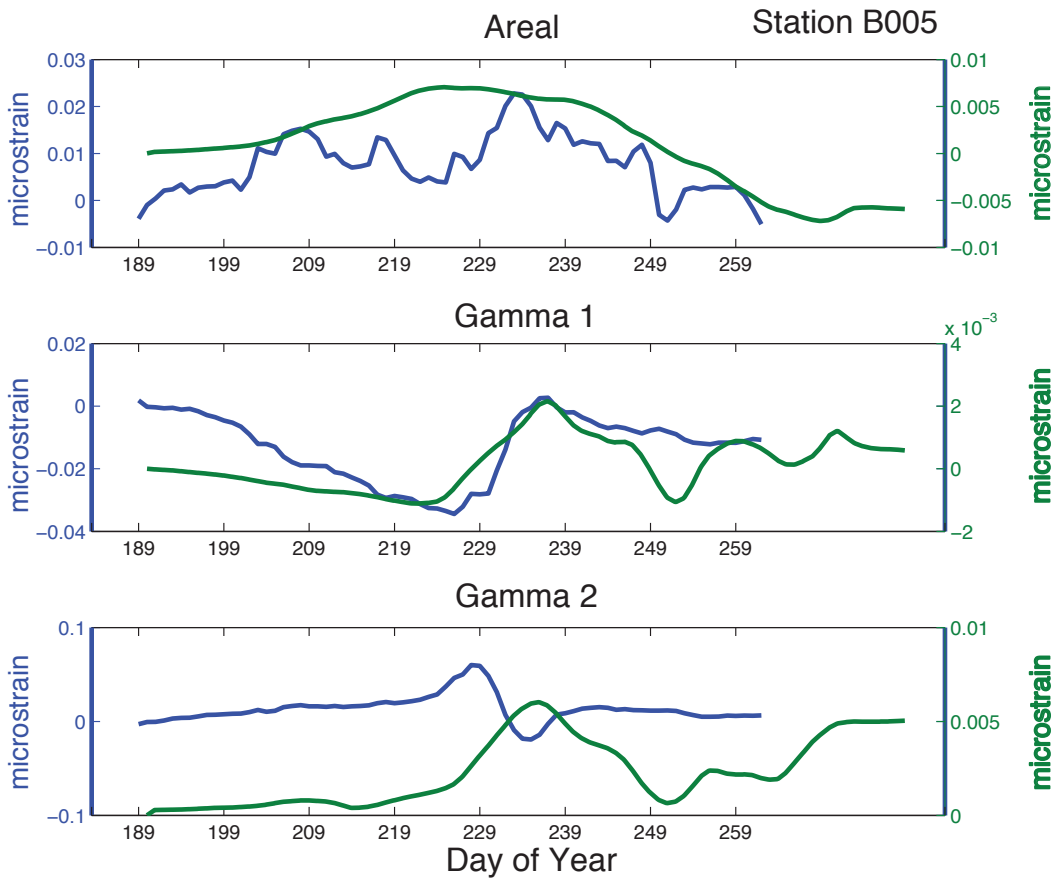

Figure 5: *Timeseries comparing GPS-predicted strain (green line) with the three components of observed transient strain (blue lines) at station B005 (near Port Angeles). The GPS-predicted strainfield approximately matches the strainmeter data for some stations, although there is a difference in scaling that may be due to the spatial and temporal smoothing of the GPS inversion results. The slow slip event is detected on several strainmeters.*

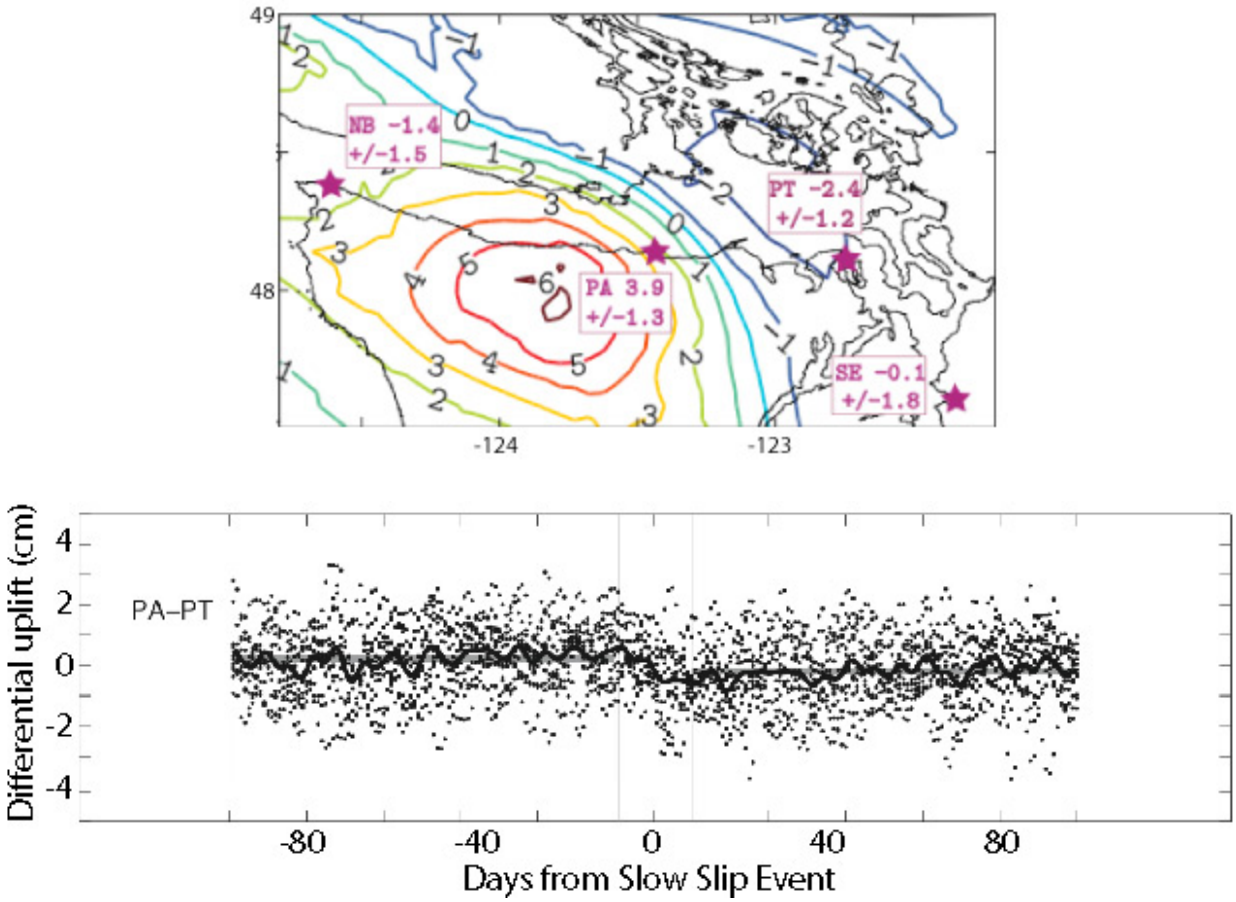

***Figure 6**: (top) A map with the location of tidal stations along the Juan de Fuca strait. Color contours show the predicted average uplift per event (mm) based on GPS-derived slip models for 11 slow slip events. The purple text shows the predicted average uplift at specific tide gauges locations. Abbreviations: NB, Neah Bay; PA, Port Angeles; PT, Port Townsend; SE, Seattle. (bottom) Stacked tide gauge time series centered on the time of a slow slip event showing the average differential uplift between Port Angeles and Port Townsend. The stack is constructed from 12 slow slip events. Tidal fluctuations and correlated ocean noise is removed leaving a small offset at the time of slow slip events. Gray bars show the average height before and after each event. The black line shows a moving average. Figures reproduced from Alba (2011).*

***Table 1:** Average differential uplift at tidal station pairs for 12 SSEs (1997-2010) compared to predictions from GPS-derived slip models.*

Station Pair	Average Differential Uplift per SSE (mm)	Predicted Differential uplift per SSE (mm)
Port Angeles – Port Townsend	-5.06±1.36	-6.24±1.76
Port Angeles – Neah Bay	-4.39±2.43	-5.21±1.98
Port Angeles – Seattle	-4.70±3.15	-3.99±2.20